Reaction Chemistry & Engineering

Multi-stage spiral-type structured catalyst system for direct large-scale methanation of industrial CO_2 emissions: A feasibility study

Journal:	*Reaction Chemistry & Engineering*
Manuscript ID	RE-ART-12-2024-000606.R1
Article Type:	Paper
Date Submitted by the Author:	24-Mar-2025
Complete List of Authors:	Akama, Hiroshi; Shizuoka University - Hamamatsu Campus Watanabe, Ryo; Shizuoka University, Verma, Priyanka; Indian Institute of Technology Delhi, Chemistry Fukuhara, Choji; Shizuoka University

ARTICLE

Received 00th January 20xx,

Accepted 00th January 20xx

DOI: 10.1039/x0xx00000x

Multi-stage spiral-type structured catalyst system for direct large-scale methanation of industrial CO_2 emissions: A feasibility study

Hiroshi Akama[a], Ryo Watanabe[a], Priyanka Verma[b],Choji Fukuhara[a,*]

The anthropogenic CO_2 emission to the atmosphere has led to severe climate changes and global warming worldwide. The conversion of CO_2 into value-added products is an important and promising solution to reduce the atmospheric levels of CO_2 and overcome the energy crisis. The CO_2 methanation reaction is being explored by many researchers and industries for the fixation of CO_2 as a power-to-gas technology. In this report, we have attempted CO_2 methanation in the presence of O_2 using a lab-scale two-stage type reactor system with Ni and Ru-based spiral-type structured catalysts. Furthermore, the thermodynamic properties of both catalysts were evaluated in the presence and absence of O_2. The combustion of H_2 due to the coexistence of O_2 promoted methanation even at room temperature conditions and showed excellent methanation performance (conv. 90% & selectivity 100%) for relatively larger amounts (5 L/min) of gas treatment. Additionally, the heat management for the reactors by adiabatic insulation was found to be effective in improving the catalytic performance and thermodynamic properties.

1. Introduction

The utilization of CO_2 by methanation is promising with respect to CO_2 capture utilization and storage (CCUS) and as power-to-gas conversion technology to mitigate the long-term energy problem[1–4]. This reaction process is attracting significant attention worldwide to produce synthetic natural gas (SNG), which can be reused as a fuel and value-added chemical[5]. However, one of the critical issues for its social implementation is to minimize energy consumption when processing large amounts of industrial exhaust gases. The exhaust gases from various industrial processes often contain O_2, for example, 3 to 13% in thermal power plants and 10% in cement plants [6]. In the conventional methanation process, the reaction is carried out under O_2-free conditions after a CO_2 separation and recovery process[7]. In the methanation reaction with the coexistence of oxygen, not only did the precious H_2 get consumed, but the concerns regarding the deactivation of the catalyst surface layer by oxidation and methane combustion to form CO_2 were argued and predicted. However, our previous studies demonstrated that the presence of O_2 only positively impacted the catalytic performance[8]. Therefore, we proposed an auto-methanation (AM) phenomenon[9] that utilizes the coexisting O_2 in exhaust gases to produce CH_4 in higher conversion and selectivity. According to AM method, the CO_2 separation and recovery process can be omitted, simplifying the operation procedure and eliminating the need for a significant initial investment in equipment. In other words, it is expected to have substantial advantages in terms of economy and efficiency. AM is also characterized by realizing a self-sustaining reaction by utilizing the heat generated by the internal H_2 combustion reaction, and hence, the reaction proceeds without any requirement for an external heat supply. The heat and gas flow management in the catalyst layer is essential for realizing a highly efficient system in this scenario. The methanation reaction (equation 1) is a typical exothermic reaction, and the H_2 combustion reaction (equation 2) included in the AM process is also highly exothermic; therefore, careful measures must be adopted to avoid the formation of hot spots in the catalyst layer. On the other hand, if the CO_2 separation and recovery process is omitted, a system that can be applied in the treatment of large amount of exhaust gases is required.

$$CO_2 + 4H_2O \rightarrow CH_4 + 2H_2O \qquad \Delta H^0_{298K} = -165 \text{ kJ·mol}^{-1} \qquad \cdots (1)$$

$$H_2 + 1/2O_2 \rightarrow H_2O \qquad \Delta H^0_{298K} = -286 \text{ kJ·mol}^{-1} \qquad \cdots (2)$$

In order to cope with the above situation, we are focusing on structured catalysts[10–12], particularly developing spiral-type structured catalysts with high heat transfer and low-pressure drop characteristics[13]. A spiral-type structured catalyst is prepared by coating the powdered sample on a substrate obtained by twisting metal plates such as aluminium or SUS (Steel Use Stainless). It is possible to control heat transfer to some extent by selecting an appropriate metal type of substrate. The Ni and Ru-based catalysts are known as typical methanation catalysts, in particular, it has been reported to display superior catalytic performances when CeO_2 was used as the support material[14–17]. We used the spiral-type structured catalysts obtained by coating the prepared powdered samples on the spiral-shaped aluminium metal plate.

[a] Department of Applied Chemistry and Biochemical Engineering, Graduate School of Engineering, Shizuoka University, 3-5-1 Johoku, Chuo-ku, Hamamatsu, Shizuoka 432-8561

[b] Department of Chemistry, Indian Institute of Technology Delhi, Hauz Khas, New Delhi – 110016, India

In this study, aiming at the social implementation of CO_2 methanation technology, we have constructed a two-stage reactor system for conducting lab-scale methanation reaction tests. The Ni- and Ru-based spiral-type structured catalysts were used, and the thermodynamic efficiency of the methanation under O_2 coexisting conditions was evaluated. Furthermore, as a thermal management of the catalyst layer, the adiabatic effect on the reaction system was also investigated without external heating.

2. Experimental

2.1. Preparation of spiral-type structured catalysts

The preparation of spiral-structured catalysts was carried out in two steps: (1) preparation of Ni and Ru-based powdered catalysts and (2) coating of these powdered catalysts onto 3-twisted spiral-shaped plates by wash-coating method. The powder catalysts of Ni/CeO_2 and Ru/CeO_2 were prepared by wet impregnation of metal precursor solution (nickel nitrate hexahydrate $Ni(NO_3)_2 \cdot 6H_2O$ and ruthenium nitrate $Ru(NO_3)_3$) onto cerium oxide (CeO_2) support, followed by evaporation to dryness and calcination for 1 h at 500 °C. The CeO_2 support material (Daiichi Kigenso Kagaku Kogyo Co., Ltd., average pore size 6.8 nm, BET surface area 126.4 m^2/g) was provided by the Catalysis Society of Japan (JRC-CEO-2). At first, the CeO_2 support powder was added to 300 mL distilled water and stirred for 12 h in vacuum at room temperature conditions. A solution of $Ni(NO_3)_2 \cdot 6H_2O$ (Wako Pure Chemical Industries, Ltd., 98%) was added to the above solution and evaporated at 80°C under continuous stirring. Then, the obtained powder was calcined in air at 500°C for 3 h to form Ni/CeO_2 catalyst. The amount of nickel loading on the CeO_2 support was fixed to 10 wt %. The Ru/CeO_2 powder catalyst was prepared by following the same procedure using ruthenium nitrate precursor solution (Tanaka Kikinzoku Kogyo K.K., 50 g L^{-1}). The ruthenium loading in the Ru/CeO_2 catalyst was also fixed to 10 wt %. The spiral-type structured catalyst was prepared by wash-coating the powdered Ni/CeO_2 or Ru/CeO_2 catalyst on a spiral-shaped plate. The spiral-shaped substrate made of aluminium has a thickness of 1.0 mm and was obtained by twisting the plate (width 11 mm and length 150 mm) three times (twist angle 1080 degrees), as shown in Fig. S1(a).

Before wash-coating the catalyst, the obtained spiral-shaped substrate was cleaned with 0.8 N NaOH solution, and the surface was activated with 2.8 M HCl solution. Then, the activated aluminium spiral substrate with a rough surface was dipped into a slurry of powder catalyst. The slurry was prepared by stirring a mixture of catalyst powder in distilled water to form a suspension. Finally, the substrate was dipped into the catalyst slurry and dried with hot air to coat the catalyst on the substrate. This dipping-drying cycle was repeated to coat 330 mg of catalyst per substrate plate, as shown in Fig. S1(b).

The Ru/CeO_2 catalyst employed in this study exhibited a Ru loading concentration of 10 wt%, which is regarded as relatively high. Nonetheless, the ruthenium concentration per unit volume of this catalyst is 2.3 g/L, a value that cannot be deemed excessive.

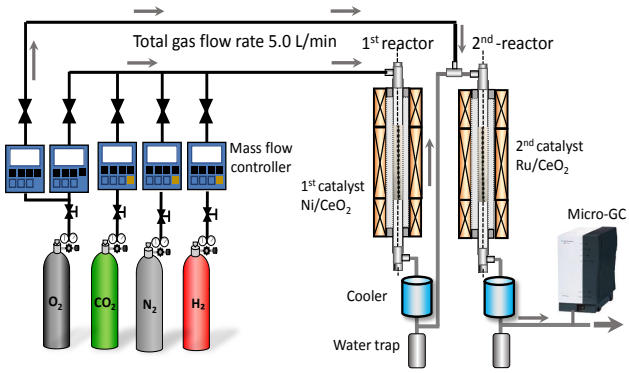

Fig. 1 The two-stage reaction apparatus system equipped with two electric furnaces.

The spiral-type catalyst is constructed from a metal plate substrate that is coated with a catalyst, facilitating relatively easy mechanical removal after the reaction. Additionally, the metal plate substrate is designed for reuse, contributing to the sustainability and efficiency of the catalytic process.

2.2. Characterization

The powder catalyst samples were characterized by several techniques, including N_2 physisorption, field emission-scanning electron microscopy (FE-SEM), X-ray diffraction (XRD), and CO_2-temperature programmed desorption (CO_2-TPD), and H_2-temperature programmed reduction studies. The specific surface area of the prepared catalyst was measured by the BET method (Micromeritics, 3Flex) using N_2 adsorption at -196 °C. The surface morphology of the prepared catalyst was observed by using FE-SEM with an energy dispersive X-ray spectrometer (EDX) (JEOL, JSM-7001F). The crystal structure for the prepared catalyst was analysed by XRD (Rigaku, Ultima Ⅳ) using CuK_α radiation. The CO_2-TPD profile and the H_2-TPR profile were measured by using MicrotracBEL's BEL-CAT instrument.

2.3. Lab-scale methanation tests

The reaction was conducted using a conventional flow-type reactor to examine the methanation performance. The external heat was uniformly supplied by a three-independent-zone electric furnace（Asahi Rika Co., ARF）controlled by a three-point PID (Proportional Integral Differential) controller. The reaction apparatus system equipped with a dual electric furnace was used, as shown in Fig. 1. Three pieces of the spiral catalyst were placed in series into a reaction glass tube (thickness: 1.5mm, internal diameter: 12mm, length: 750mm) and installed in the electric furnace. The Ni/CeO_2 catalyst was placed in the first reactor, and the Ru/CeO_2 catalyst was placed in the second reactor. The Ni-based catalyst is comparatively excellent in heat resistance and cost-effective properties, so it has many advantages as a practical catalyst, and was placed on the front stage side where the catalyst is exposed to more severe conditions. On the other hand, the more expensive Ru-based catalyst is highly active but has weaker heat resistance, so it was placed in the latter stage.

Table 1 Loading amount of catalyst metal, BET surface area, and crystallite size of metal for Ni/CeO_2 and Ru/CeO_2 catalyst.

Catalyst	Loading amount of catalyst metal / wt%	BET surface area / $m^2 \cdot g^{-1}$-cat		Crystallite size of metal / nm	
		As prepared 500 °C in air	After H_2 reduction 500 °C 1hr	As prepared 500 °C in air	After H_2 reduction 500 °C 1hr
Ni/CeO_2	10	114.8	94.2	28 NiO (111)	22 Ni (111)
Ru/CeO_2	10	123.3	113.3	42 RuO_2 (101)	21 Ru (101)

The flow rate of the reaction gas was 5.0 L/min, and the O_2 concentration at the inlets of the first and second reactors was set to 5 vol% and 0 to 3 vol%, respectively, considering practical conditions. In this case, GHSV (Gaseous Hourly Space Velocity) per reactor was 7,000 h^{-1}, LV(Linear Velocity) was 880 mm/sec, and contact time was 0.51 sec. A K-type thermocouple was used to measure the temperature of the catalyst during the reaction at three different points: the catalyst inlet tip (inlet), the catalyst outlet tip (outlet), and the reaction tube outer wall at the catalyst bed center (center).

The gas composition was $CO_2 : H_2 = 1 : 5$ to 5.6 (corresponding to H_2 stoichiometry); the remaining was N_2 gas. The catalysts were reduced by H_2 stream of 100 mL/min at 500°C for 2h for the first reactor catalyst (Ni) and 200°C for 2h for the second reactor catalyst (Ru) before the reaction. Then, the CO_2 methanation test was carried out by introducing feed gas to the reactor at the setting furnace temperature of 350°C or 300°C, and then the temperature was lowered step by step towards 25°C (room temperature). The gas composition at the first and second reactor outlets were analyzed with a micro gas chromatograph (Agilent 490 Micro GC) equipped with a thermal conductivity detector (TCD).

The CO_2 conversion and CH_4 selectivity were calculated using equations (3) and (4), respectively.

$$CO_2 \text{ conversion}(\%) = \frac{F_{CO_2,inlet} - F_{CO_2,outlet}}{F_{CO_2,inlet}} \times 100 \quad \cdots \quad (3)$$

$$CH_4 \text{ selectivity}(\%) = \frac{F_{CH_4,outlet}}{F_{CO_2,inlet} - F_{CO_2,outlet}} \times 100 \quad \cdots \quad (4)$$

The amount of CO_2 in equations (3) and (4) was determined directly from the experimental values, utilizing N_2 as an internal standard.

2.4. Exergy evaluation

Based on the reaction results, the standard exergy and physical exergy were calculated by the following equations (5) and (6), respectively.

$$\text{Standard exergy } \varepsilon^0 = \sum_i y_i \cdot \varepsilon_i^0 + R\,T_0 \sum_i y_i \cdot \ln(P_i) \quad \cdots \quad (5)$$

$$\text{Physical exergy } \varepsilon_p = \Delta H - T_0 \Delta S = \int_{T_0}^{T} \sum_i y_i \cdot C_{p,i}\, dT \quad \cdots \quad (6)$$

The exergy efficiency of produced CH_4 (η_{CH4}) defined by the following equation (7) was used as an efficiency index of exergy.

$$\eta_{CH_4}(\%) = \frac{\text{Exergy(Produced } CH_4)}{\text{Exergy(Feeding materials)+Input power}} \times 100 \quad \cdots \quad (7)$$

Where, the input power is the external heating energy by the electric furnace.

3. Results and Discussion

3.1. Characterization of catalysts

Table 1 shows the loading amount of metal and the BET surface area before and after H_2 reduction at 500°C for Ni/CeO_2 and Ru/CeO_2 catalysts. It also includes the crystallite diameters of Ni and Ru particles determined by Scherrer equation from the XRD profiles shown in Fig. 2. The BET surface areas of the catalysts decreased after H_2 reduction at 500°C. Specifically, the decrease in BET surface area for the Ni catalyst was 20%, while for the Ru catalyst, it was 10%. Interestingly, the decrease in BET surface area was even more suppressed in the latter catalyst. After H_2 reduction, the crystallites of Ni and Ru particles in the catalysts became smaller in size. In particular, the diameter of the Ru crystallite was reduced by half. It

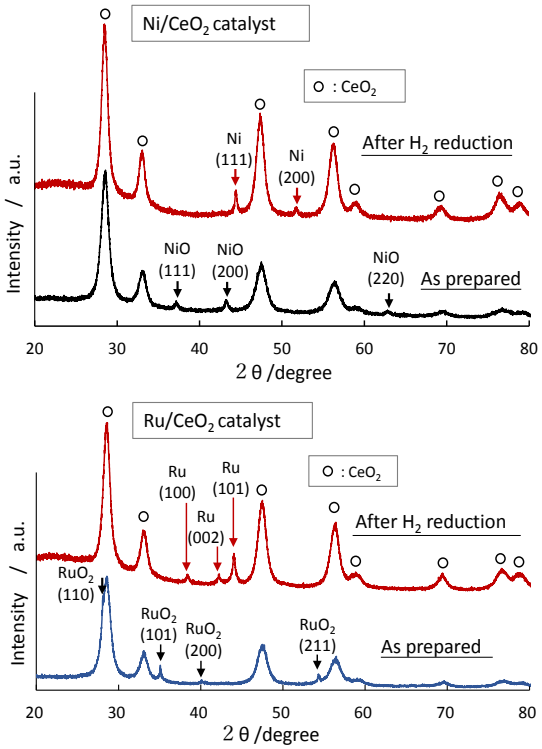

Fig. 2 XRD profile of Ni/CeO_2 and Ru/CeO_2 catalyst before and after H_2 reductions.

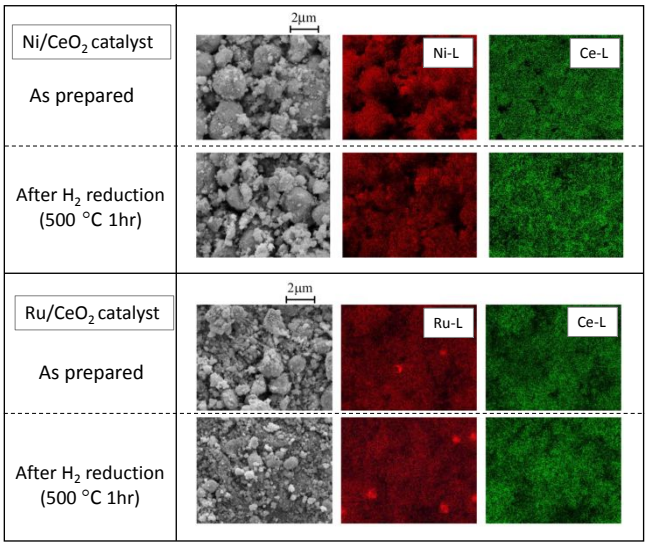

can be suggested that H_2 reduction uniformly disperses the metal

Fig. 3 Surface morphology and element mapping of before and after reduction for Ni/CeO_2 and Ru/CeO_2 catalyst by SEM-EDX.

nanoparticles on the support. One possible reason for the suppression of BET surface area decrease in the Ru/CeO_2 catalyst after H_2 reduction is the redispersion of Ru particles on the CeO_2 support, caused by strong interaction between Ru and CeO_2.

Fig. 3 shows the surface morphology and elemental mapping images of Ni/CeO_2 and Ru/CeO_2 catalysts obtained by SEM-EDX before and after H_2 reduction at 500°C. The images show that Ni or Ru nanoparticles are dispersed on the catalyst surface, and these particles tend to be reduced in size by the reduction process. This is more obvious with the Ru catalyst and matches the change in crystallite diameter, as determined by XRD measurements.

Fig. 4 shows the reduction properties of the catalyst and CeO_2 support by H_2-TPR analysis. Each sample was oxidized at 300°C for 1 h in air and cooled to room temperature. The H_2 consumption was then measured by TCD by heating from 0°C to 800°C at a rate of 10°C/min in H_2 (4 vol%)/N_2 mixture flow. The H_2-TPR profile of the Ru/CeO_2 catalyst showed the existence of three types of Ru that are easily reduced at lower temperatures below 200°C. The peaks in the low-temperature range are attributed to small-sized Ru nanoparticles with uniform dispersion on the CeO_2 support, and the peak on the high-temperature side is attributed to relatively large Ru particles. Based on this observation, the H_2 reduction temperature for pretreatment was set to 200°C.

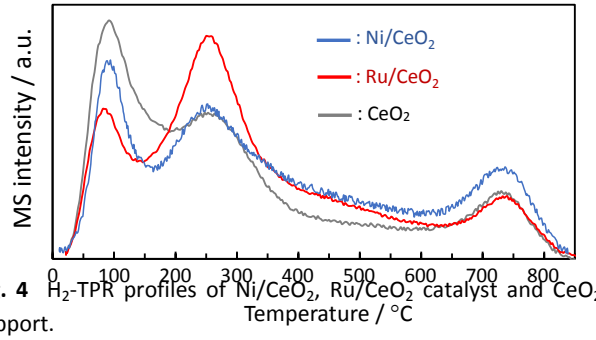

Fig. 4 H_2-TPR profiles of Ni/CeO_2, Ru/CeO_2 catalyst and CeO_2 support.

On the other hand, in the Ni/CeO_2 catalyst profile, peaks attributed to two types of Ni nanoparticles appeared at 257°C and 350°C. A temperature of at least 450°C is required to reduce Ni nanoparticles in the catalyst completely. Therefore, the H_2 reduction temperature for pretreatment was set to 500°C.

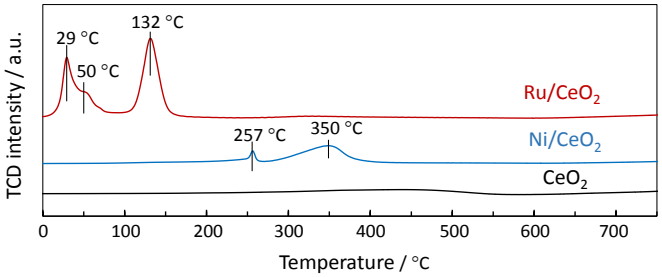

Fig. 5 CO_2-TPD profiles of Ni/CeO_2, Ru/CeO_2 catalyst and CeO_2 support.

Fig. 5 shows the CO_2 desorption properties of the prepared catalysts and CeO_2 support. Each sample was subjected to H_2 reduction at 500°C for 1 h, and then CO_2 was adsorbed by flowing CO_2 (1 vol%)/He gas at 50°C. Next, the amount of CO_2 (m/z=44) desorbed was measured using a mass spectrometer by heating from 20°C to 800°C at 10°C/min in He gas flow conditions. Three types of CO_2 desorption peaks were observed in the profile of all samples, with peaks at temperature around 100°C, 200-350°C, and around 750°C. These peaks are attributed to represent the base strength of the active sites on the surface of catalyst. Since the methanation reaction progresses at temperature of above 200°C, it is presumed that CO_2, desorbed in the temperature range of 200 to 350°C, is involved in the methanation reaction. By supporting Ru on the CeO_2 support, the amount of CO_2 desorption at around 100°C decreased, and the amount of CO_2 desorption from 200 to 350°C significantly increased. The obtained results justify the high catalytic activity of Ru-based catalysts. The Ni catalyst was found to have similar, although less pronounced, properties. In the two-stage catalyst system, by placing a more active Ru-based catalyst in the latter stage, we expected to convert CO_2 that was not completely consumed in the first stage with higher efficiency.

3.2. Catalytic performance

The lab-scale test results of conventional methanation reaction, namely, without oxygen co-feeding, under the gas flow rate of 5.0 L/min, are shown in Fig. 6. The experimental operation started at 350°C, and the setting temperature was lowered step by step towards room temperature. As shown in Fig. 6 (a), at the setting temperature of 350°C, a high CO_2 conversion of over 90% was obtained at the second reactor outlet, which exceeded the equilibrium value. However, at temperature below 300°C, the CO_2 conversion was drastically decreased, and no reaction occurred at temperature below 200°C. On the other hand, with the Ni-based system (first reactor), a setting temperature of 300°C is required to obtain CO_2 conversion exceeding 50%.

The combination of first reactor (Ni-based) with the Ru-based catalyst in the second reactor exceeded the CO_2 conversion to 60%

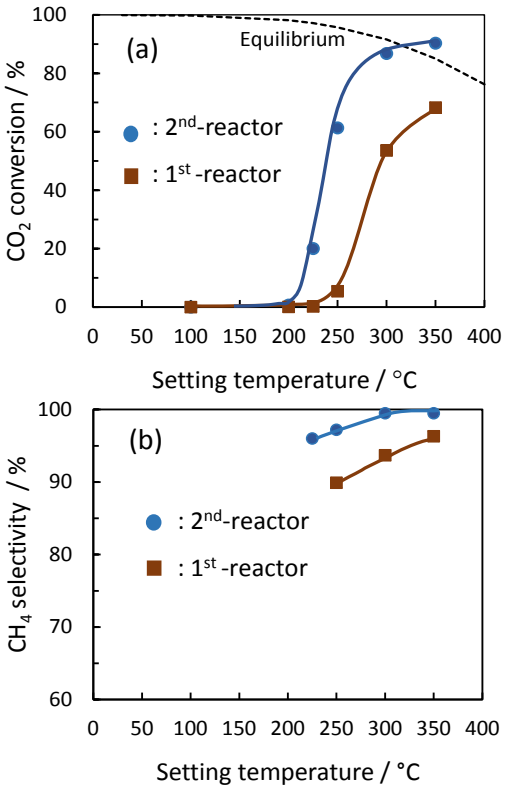

Fig. 6 (a) CO_2 methanation performance and **(b)** CH_4 selectivity of two-stage reactor system under the conventional condition i.e., without oxygen co-feeding.

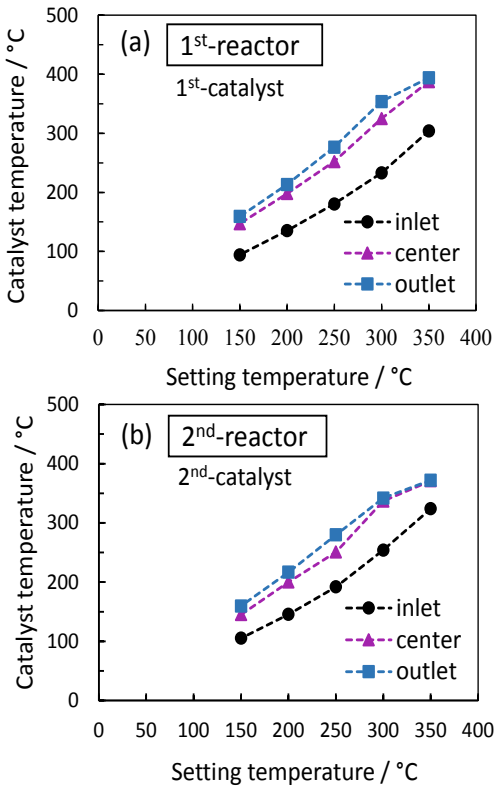

Fig. 7 Relationship between the setting temperature and the catalyst temperature (3 parts) of **(a)** the first reactor and **(b)** the second reactor of two-stage reactor system under the conventional condition i.e., without oxygen co-feeding.

at the setting temperature of 250°C, 87% at 300°C, and more than 90% at 350°C, exceeding the equilibrium value. Furthermore, as shown in Fig. 6 (b), the CH_4 selectivity was also improved by the combination of Ni with Ru-based catalyst, and hence, the effect of the two-stage reaction system was found to be remarkable in enhancing the overall catalytic performance. The effect of the two-stage system on obtaining CO_2 conversion above equilibrium was attributed to the function of the intermediate water trap. In addition, it is considered that the application of a spiral-type structured catalyst made of aluminum has excellent thermal conductivity, which assists in suppressing overheating of the catalyst layer [13].

Fig. 7 represents the relationship between the setting and catalyst temperatures (3 different points) of the first and second reactors. Both catalysts in two reactors have profiles with lower inlet temperatures and higher outlet temperatures. The inlet temperature of the first and second reactor catalysts showed almost similar characteristics and was lower than the setting temperature. This is because the gas was not preheated, so a cooling effect acts at the inlet of the catalyst layer. When the feed gas was heated inside the catalyst layer, a reaction occurs, and the heat of the reaction raises the temperature of the catalyst layer above the setting temperature. This behavior was observed at the outlet temperature.

The CO_2 conversion of the first reactor catalyst at the setting temperature of 350°C was 68.3%. At this time, the temperatures at the outlet end of the catalyst and the center of the outer wall of the reaction tube were 394°C and 388°C, respectively. That is, the maximum temperature inside the catalyst layer is about 390°C. The CO_2 conversion (68.3%) in the single reactor does not reach the equilibrium conversion of 78.0% at 390°C. Since the H_2O generated in the first reactor was trapped before feeding the gases into the second reactor, the reaction in the second reactor gets promoted, and the two-stage reactor as a whole system achieves a CO_2 conversion of 90.3%, which exceeds the equilibrium value (78.0%).

As shown in Fig. 7, the temperature difference between the inlet and outlet of the catalyst layer of the first and the second reactor at the setting temperature of 350°C is smaller than at the setting temperature of 300°C. In particular, an increase in the catalyst outlet temperature at 350°C was found to be suppressed. We predict that the excellent heat transfer ability of the structured catalyst contributes to the suppression of overheating of the catalyst layer.

Fig. 8 represents the CO_2 methanation performance in the presence of O_2. From the inlet of the first reactor, 5 vol % of O_2 was supplied, and the amount of O_2 supplied from the inlet of the second reactor was varied from 0 to 5 vol %.

The explosion limits of H_2 in air range from 4.0 to 75.0 vol%. Therefore, the conditions of this experiment fall within this range. Additionally, the concentration of O_2 is crucial for H_2 explosions. It is generally accepted that an explosion may occur when the O_2 concentration exceeds 5 to 6 vol%. However, it has been confirmed

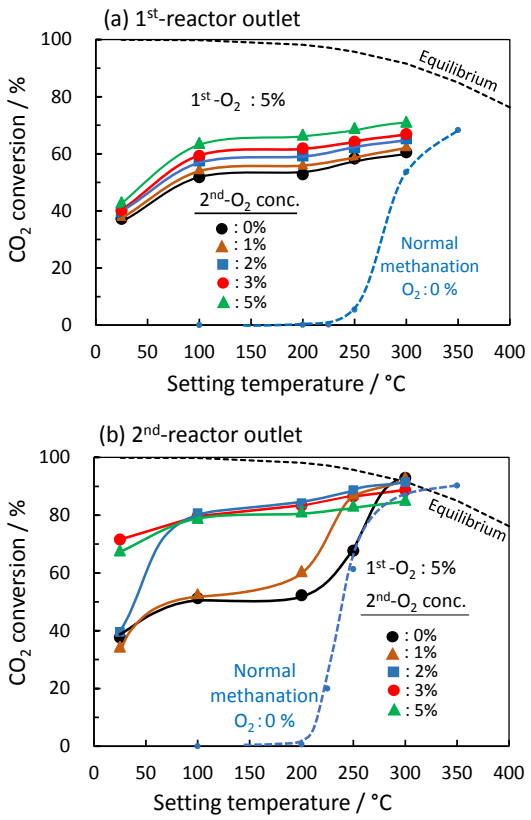

Fig. 8 (a) CO_2 methanation performance of first reactor under O_2 coexistence condition, **(b)** CO_2 methanation performance of two-stage reactor system under O_2 coexistence condition.

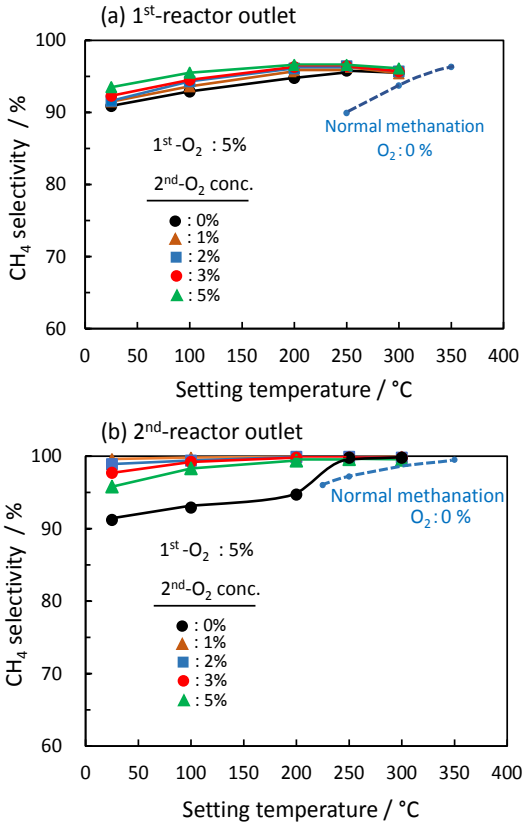

Fig. 9 CH_4 selectivity of **(a)** first reactor and **(b)** second reactor under various O_2 conditions.

that no H_2 explosion occurs at an O_2 concentration of 5 vol% in the context of this experiment.

The CO_2 conversion at the outlet of the second reactor is shown in Fig. 8 (b). The obtained value corresponds to the CO_2 conversion of a two-stage reactor system. In this case, the experimental operation was started at 300°C, and the setting temperature was lowered stepwise towards room temperature conditions. At a setting temperature of 300°C, the lower O_2 concentration in the second reactor resulted in a higher CO_2 conversion. The CO_2 conversion at an O_2 concentration of up to 3 vol% was higher than that of conventional methanation without O_2. However, when the O_2 concentration in the second reactor was 5 vol% , the CO_2 conversion was slightly lower than that of conventional methanation. The coexistence of O_2 dramatically enhanced CO_2 conversion in the temperature range below 200°C compared to conventional methanation.

The introduction of O_2 raises concerns regarding potential side reactions, including the combustion of H_2 and the combustion of generated CH_4. However, H_2 possesses a minimum ignition energy that is less than approximately 1/15 of that of CH_4, resulting in preferential combustion of H_2. This reaction primarily occurs at the tip of the catalyst inlet, where O_2 is entirely consumed. The heat generated from this combustion diffuses along the gas flow throughout the catalyst, thereby promoting CO_2 methanation. The high thermal conductivity of the spiral catalyst further enhances this process. Consequently, significant side reactions that could disrupt the equilibrium are minimized. On the other hand, the H_2O produced from H_2 combustion does influence the equilibrium and adversely affects CO_2 methanation. In fact, increasing the O_2 concentration tends to decrease CO_2 conversion, as demonstrated at 300℃ in Fig. 8(b). Nevertheless, the heat generated from H_2 combustion raises the temperature of the catalyst layer, which promotes the reaction and mitigates the negative impact of H_2O. As a result, at an O_2 concentration of 3 vol%, the effect of heat generation on reaction promotion becomes dominant.

In the two-stage reactor system, at the conditions of the second reactor O_2 concentration of 3 vol% and 5 vol%, a higher CO_2 conversion level was maintained even at room temperature without external heating. We named this phenomenon 'auto-methanation' [9], in which the methanation reaction self-sustains without needing external heating. At the second reactor with an O_2 concentration of 3 vol%, CO_2 conversion of more than 70% was obtained under room temperature conditions. This excellent performance was due to the suppression of excessive temperature rise in the catalyst layer, facilitated by the dissipation of reaction heat based on the high thermal conductivity of the structured catalyst and the equilibrium shift effect caused by the generated water trap in the middle of the two-stage system.

The effectiveness of the two-stage reactor system can be understood from the methanation characteristics of the first reactor shown in Fig. 8(a). When 5 vol% O_2 coexists in the inlet gas of the first reactor, CO_2 methanation proceeds even when the set temperature is below 250°C. When the inlet O_2 concentration in the second reactor is 5 vol%, the CO_2 conversion rates at set temperatures of 200°C, 100°C, and room temperature are 66.7%, 63.8%, and 43.0%, respectively. These results indicate that the coexisting O_2 enhances catalyst performance and enables the auto-methanation phenomenon.

The amount of H_2 supplied to the inlet of the first reactor includes the H_2 equivalent corresponding to the O_2 supplied to the second reactor. Consequently, the H_2/CO_2 ratio at the inlet of the first reactor increases with the amount of O_2 fed into the second reactor. For instance, the H_2/CO_2 ratios at the inlet of the first reactor, under conditions where the O_2 concentration in the second reactor is 1 vol%, 2 vol%, 3 vol%, and 5 vol%, were measured at 4.2, 4.4, 4.6, and 5.0, respectively. Thus, the H_2/CO_2 ratio at the inlet of the first reactor is influenced by the O_2 supply concentration to the second reactor, which in turn affects the H_2/CO_2 ratio at the outlet of the first reactor. When the O_2 supply concentration to the second reactor is elevated, the H_2/CO_2 ratio at the inlet of the first reactor increases, resulting in a higher CO_2 conversion in the first reactor.

From Fig. 8(a), the CO_2 conversion in the single-stage catalyst at an O_2 concentration of 3 vol% is 59.3% and 40.1% at the setting temperatures of 100°C and room temperature, respectively. In contrast, from Fig. 8(b), the CO_2 conversion in the two-stage catalyst at the same O_2 concentration of 3 vol% and the same setting temperatures is improved to 78.7% and 71.6%, respectively. This significant improvement can be attributed to the equilibrium shift effect of the intermediate H_2O trap in the two-stage catalytic reactor system. Furthermore, the CO_2 conversion in the two-stage catalytic reactor system varies with the amount of O_2 fed to the second reactor inlet, with the highest CO_2 conversion observed when the O_2 concentration in the second reactor is 3 vol%.

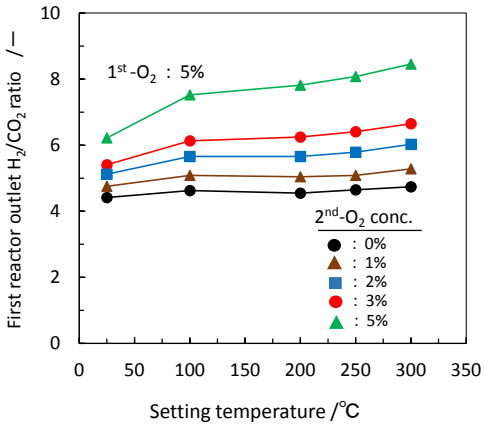

Fig. 10 H_2/CO_2 ratio at the outlet of the first reactor.

Fig. 10 shows the H_2/CO_2 ratio at the outlet of the first reactor. This ratio is a crucial factor related to the CO_2 conversion and CH_4 selectivity. As mentioned earlier, the amount of H_2 supplied from the inlet of the first reactor corresponds to the O_2 supply concentration to the second reactor. Consequently, the H_2/CO_2 ratio tends to increase with higher O_2 supply concentrations to the second reactor. A higher oxygen supply concentration leads to an increase in the amount of H_2O produced, which inhibits the reaction. However, this inhibition is compensated for by increasing the H_2/CO_2 ratio, resulting in an improved CO_2 conversion rate, partly due to the temperature-raising effect of the catalyst layer. Therefore, even when the oxygen supply concentration to the second reactor is as high as 5 vol%, a high CO_2 conversion rate can still be achieved.

The positive effect of splitting the reactor into two stages was also observed in the CH_4 selectivity, as shown in Fig. 9 (a) and (b). The maximum CH_4 selectivity at the outlet of the first reactor was 97% in

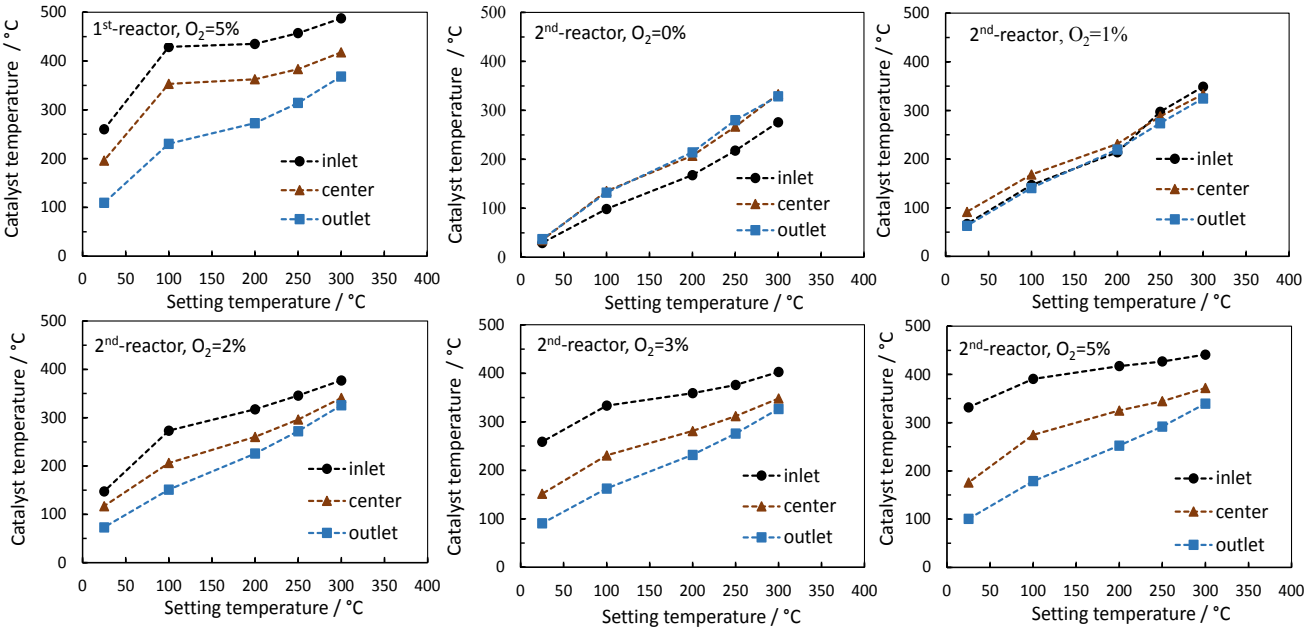

Fig. 11 Relationship between setting temperatures and catalyst temperatures.

the temperature range from room temperature to the setting temperature of 300°C. On the other hand, CH_4 selectivity at the second reactor with an O_2 concentration of 3 vol% exceeded 98% even under room temperature conditions.

The reaction characteristics of this two-stage reactor system can be understood from the temperature profile of the catalyst layer shown in Fig. 11. When O_2 (5 vol%) was supplied to the first reactor, the temperature of the catalyst inlet was increased due to H_2 combustion, and the heat propagates to the rear side of the catalyst layer, raising the temperature of the entire catalyst layer. This reactor does not have the function of preheating the reaction gas, but the H_2 combustion at the inlet part of the catalyst plays the role of preheating. From the temperature profile of the first reactor, the catalyst inlet temperature was increased to nearly 500°C and the outlet temperature reached 370°C at the setting furnace temperature of 300°C. As the temperature of the catalyst layer rises, the CO_2 conversion decreases due to the equilibrium constraint. However, the spiral-type structured catalyst based on an aluminum metal substrate has excellent heat transfer ability, and it is speculated that the spiral shape, which has a relatively larger aspect ratio of length to diameter, enables effective treatment of CO_2 in a wide range of temperature profile conditions. In addition, the temperature profile of the first reactor was hardly affected by the supplied O_2 concentration conditions of the second reactor.

As shown in Fig. 6 (a), a temperature above 250°C is required to activate the first reactor with Ni/CeO_2 catalyst. The inlet temperature of the catalyst layer was 260°C at room temperature with coexisting oxygen without external heating, so the first reactor catalyst was activated, and the reaction proceeded. On the other hand, the activation of the second reactor with Ru/CeO_2 catalyst requires a temperature of above 200°C.

In the second reactor catalyst, when the O_2 concentration was 1 vol%, the effect of increasing the temperature of the catalyst layer due to H_2 combustion was insufficient, and the setting temperature of 250°C was required to activate the catalyst. When the second reactor O_2 concentration was 2 vol%, the H_2 combustion effect appeared at the setting temperature of 100°C, but at room temperature, the inlet temperature rose only up to 150°C, so the catalyst was not activated. However, in the case of 3 vol % O_2 concentration, the inlet temperature of the catalyst layer rises to 260°C even at room temperature, so the catalyst was activated. Since the electric furnace is turned off and left open at room temperature, an image of the temperature profile of the catalyst layer can be observed using an infrared (IR) camera, as shown in Fig. 12 (a). When observing the temperature of the catalyst layer with an IR camera, the transmittance was adjusted based on the temperature of the thermocouple installed at the inlet of the catalyst. As shown in Fig. 12(a), in the first reactor, 3 pieces of catalysts were used, and the temperature profile clarified that the 3rd catalyst was not activated. On the other hand, in the second reactor, only the first piece of the catalyst was activated. That is, only half of the catalysts contribute to the reaction under these conditions. Fig. 11 (b) shows the temperature profile of the catalyst layer obtained from the data of the IR camera. It can be seen that the temperature of first catalyst in the first reactor reaches its maximum slightly downstream from the inlet and then gradually decreases towards the outlet. The catalyst is fully activated at temperatures above 250°C (red dotted line). The maximum temperature of the catalyst layer in the first reactor, which has a higher O_2 concentration, exceeds 500°C, and the temperature range exceeding 250°C covers almost 80% of the second catalyst layer. The maximum temperature of the catalyst layer in the second reactor is 400°C, and the temperature above 250°C is 90% of the first catalyst layer and less than 30% of the second catalyst layer. A notable feature of this spiral-type structured catalyst is its high heat

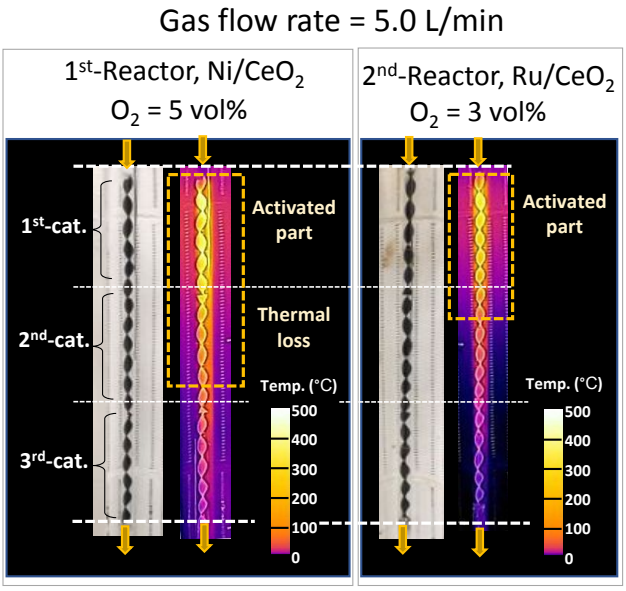

Fig. 12 (a) Thermal images of two-stage spiral-type structured catalysts.

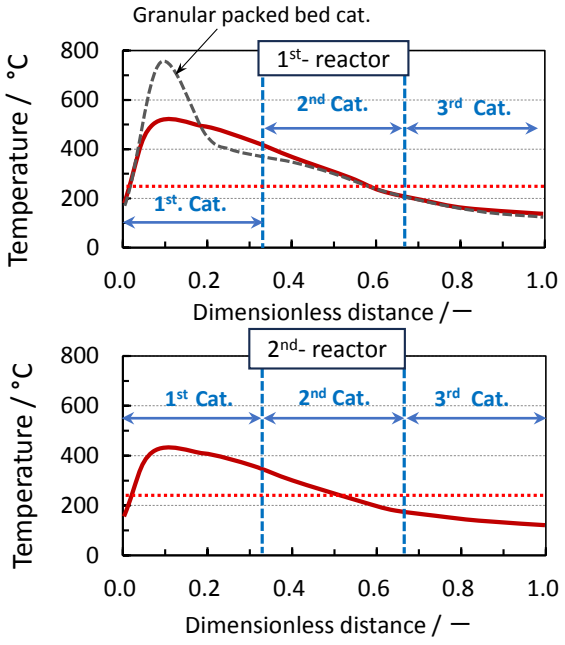

Fig. 12 (b) Temperature profiles of the two-stage spiral-type structured catalyst layer.

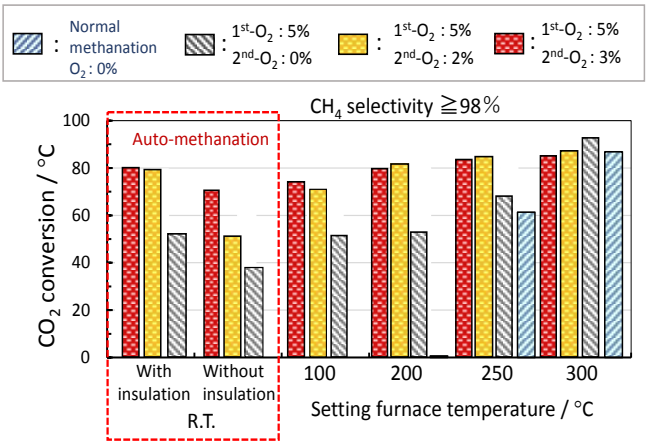

Fig. 13 Catalyst performance of two-stage reactor with insulation treatment.

conductivity, which suppresses excessive temperature rise and prevents the formation of hot spots. In Fig. 11 (b), the temperature profile (black dashed line) of the packed granular catalyst is shown as a reference. Granular catalysts have a high heat storage effect, which can cause the temperature near the catalyst inlet to increase significantly due to H_2 combustion heat, leading to thermal runaway. Spiral structure catalysts offer a superior solution to this problem.

At this time, the IR-image photo indicates that the temperature around the reaction tube was also increased. This means that heat is released in the radial direction of the reaction tube at room temperature, and the heat of H_2 combustion and methanation reaction is not fully utilized.

As a heat management strategy of the catalyst layer to eliminate this heat loss, as shown in Fig. S2, heat insulation (alkaline earth silicate) was wrapped around the reaction tube to control the heat dissipation from the catalyst layer.

Fig. 13 represents the CO_2 conversion when heat insulation was applied to the reaction tube. The O_2 conditions were 5 vol% for first reactor and 2 vol% or 3 vol% for second reactor. By this insulation treatment, CO_2 conversion remarkably improved and reached 80% under any O_2 concentration, and CH_4 selectivity exceeded 98%. This characteristic is comparable to the performance at a setting temperature of 200°C. In other words, this means that the amount of heat equivalent to 200°C by an electric furnace could be reduced. According to the temperature profile of the catalyst under each condition shown in Fig. 13, the temperature at the catalyst inlet was increased to 300°C in the first reactor due to adiabatic treatment, and the temperature at the center of the outer wall of the reaction tube reached the same level as the condition of setting temperature of 300°C. Furthermore, the temperature at the center of the outer wall of the reaction tube showed almost the same temperature as the 250°C setting temperature with 3 vol% O_2 concentration and rose to the same level as the 200°C setting temperature at 2 vol% O_2 concentration.

On the other hand, as shown in Fig. 6 (a), without O_2, the reaction hardly occurred even at the electric furnace setting of 200°C, and the electric furnace setting temperature above 250°C is required to obtain over 80% of CO_2 conversion. It is understood that the effect of internal heat supply by H_2 combustion at the catalyst layer is the effect of the coexistence of O_2, which makes external heat supply by an electric furnace unnecessary. This observation clearly explains the

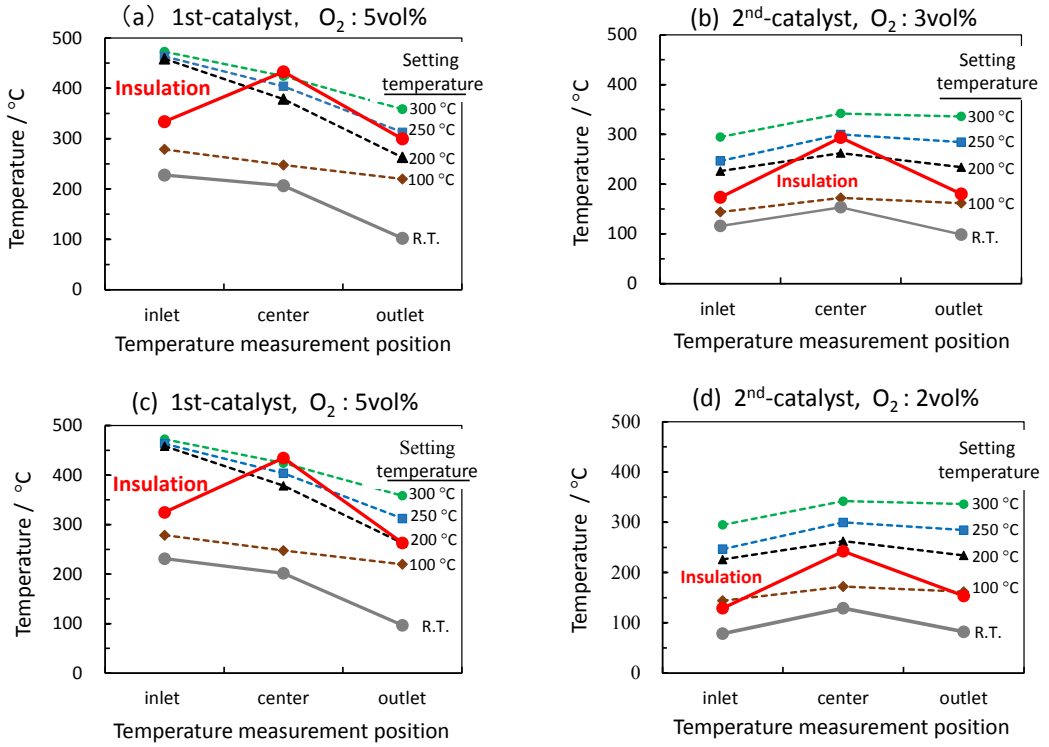

Fig. 14 Temperature profiles of the catalysts in various O_2 and setting temperature conditions (a) first catalyst with 5 vol % O_2, (b) second catalyst with 3 vol % O_2, (c) first catalyst with 5 vol % O_2 and (d) second catalyst with 2 vol % O_2 .

effect of auto-methanation.

3.3. Exergy evaluation

In order to understand which method is more efficient, internal heating or external heating, we have calculated the thermodynamic efficiency using the exergy index. Standard exergy and physical exergy shown by equation (5) and (6) were calculated, and the exergy efficiency of produced CH_4 (ηCH_4) defined by equation (7) was used as an index of the exergy efficiency. Here, the input power in equation (7) is the heat supplied from the outside, which is the heating energy from the electric furnace. But now, the question arises about how this value can be obtained. For example, when the temperature of an electric furnace was set to 200°C, it included raising the temperature to 200°C and maintaining the same at 200°C. That is, heating the catalyst layer by the electric furnace requires the energy for raising the temperature of the electric furnace body to 200°C and the energy for maintaining the temperature of 200°C.

Therefore, the average power consumption of the electric furnace during the process of heating up to the setting temperature and holding at that temperature was measured. The average power consumption was determined from the resistance value of the electric furnace and the current value measured every minute during both the heating and holding processes.

Fig. 15 shows the relationship between the setting furnace temperature and the average power consumption of two electric furnaces.

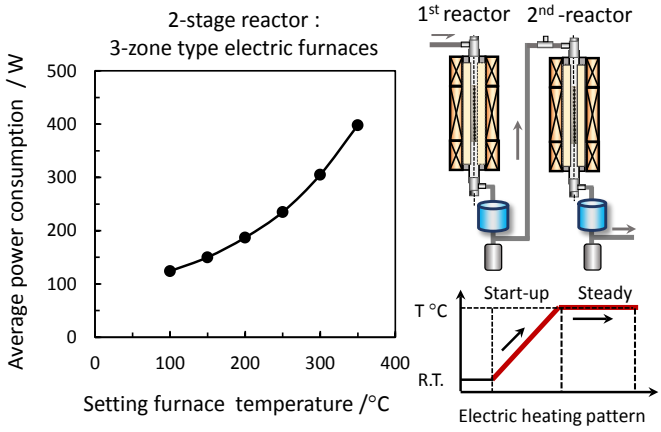

Fig. 15 Average power consumption of electric furnace.

Based on the above performance evaluation results and the electric furnace's average power consumption, the produced CH_4 (η_{CH4}) exergy efficiency in Equation (7) was calculated. Fig. 16 shows the values of exergy efficiency of produced CH_4 (η_{CH4}) for the conventional methanation (without O_2, with electric heating) and the methanation with O_2 coexistence condition (i.e., auto-methanation). The η_{CH4} value of conventional methanation was up to 41% at a setting temperature of 300°C. In contrast, η_{CH4} value of auto-methanation at room temperature reached 45%. Further, applying the heat-insulating treatment to the reaction tube under room temperature conditions, the ηCH_4 value of auto-methanation was significantly improved by up to 52%. It can be seen that the effect of heat insulation treatment on improving efficiency was remarkable.

Another important point is that conventional methanation does not react well below 200°C, so external heat is required, and the associated CO_2 production cannot be ignored. The amount of CO_2 produced based on the CO_2 emission factor (0.441kg-CO_2/kWh: Japan average for FY2020) from the average power consumption of electric furnace heating is also shown in Fig. 15. More than 1.0 L/min of CO_2 was produced at the setting temperature of 300°C, which has a negative impact on its η_{CH4} values. By contrast, in the case of auto-methanation, which utilizes the internal heat supply method using H_2 combustion, there is no CO_2 production by electric heating, and more than 50% of η_{CH4} was obtained by applying adiabatic treatment to

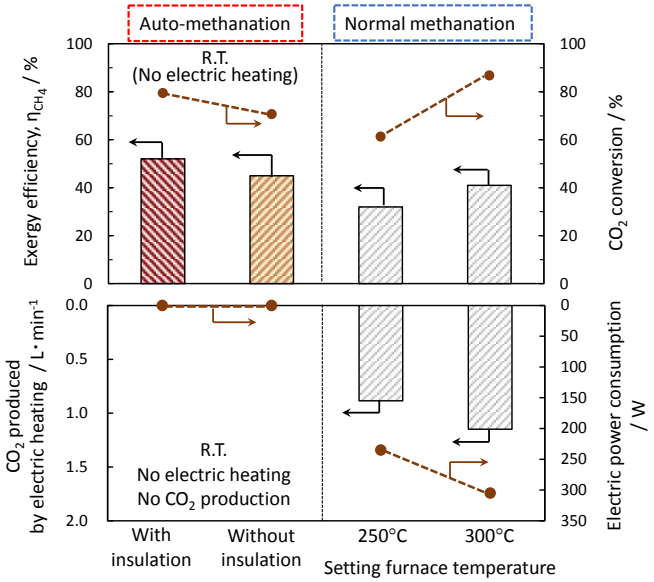

Fig. 16 Exergy efficiency of produced CH_4 (η_{CH4}) (upper graph) and amount of produced CO_2 by electric heating (lower graph) , Comparing with auto-methanation and normal methanation.

the reaction tube at room temperature conditions.

4. Conclusions

The lab-scale two-stage catalyst reactor system incorporating Ni- and Ru-based spiral-type structured catalysts showed excellent methanation performance for a relatively large amount of CO_2 gas treatment by applying the auto-methanation method in which heat of H_2 combustion was utilized for internal heating. Furthermore, it was found that performance and exergy efficiency can be effectively improved by applying thermal management to the reactor by adiabatic treatment. As a result, exhaust CO_2 can be treated with high efficiency under practical conditions of GHSV:7,000 h^{-1} and a contact time of 0.5 seconds. Conventional methanation requires external heating, and if additional CO_2 is generated by the heating, it will have a negative impact on the CO_2 reduction effect. On the other hand, auto-methanation consumes H_2 but does not cause additional CO_2 generation. If it becomes possible to further reduce H_2 consumption with the auto-methanation method, it will be

possible to obtain a significant cost advantage, and it is expected to open the way to the realization of the social implementation of this technology.

Nomenclatures

$F_{CO2,inle}$: molar flow rate of CO_2 at the reactor inlet
$F_{CO2,outlet}$: molar flow rate of CO_2 at the reactor outlet
$F_{CH4,inlet}$: molar flow rate of CH_4 at the reactor outlet
$F_{CO,\ outlet}$: molar flow rate of CO at the reactor outlet
ε^0 : Standard exergy
ε_p : Physical exergy
y_i : Molar ratio of component i
P_i : Partial pressure of component
$\varepsilon_{\ i}{}^{o}$: Standard exergy of component i
$C_{p,i}$: Molar specific heat capacity of component i at constant pressure

Conflicts of interest

There are no conflicts to declare.

Acknowledgement

This work was supported by JST-ALCA-Next Program Grant Number JPMJAN24C2, Japan.

References

1. S. Schiebahn, T. Grube, M. Robinius, V. Tietze, B. Kumar, D. Stolten, *Int J Hydrogen Energy*, 2015, **40**, 4285–4294.
2. A. Lewandowska-Bernat, U. Desideri, *Appl Energy*, 2018 **228**,57–67.
3. A. Vita, C. Italiano, L. Pino, P. Frontera, M. Ferraro, V. Antonucci, *Appl. Catal. B*, 2018, **226**, 384–395..
4. M. Thema, F. Bauer, M. Sterner, Power-to-Gas, *Renewable and Sustainable Energy Reviews*, 2019 , **112** ,775–787.
5. M.D. Porosoff, B. Yan, J.G. Chen, Energy Environ Sci., 2016 **9** , 62–73.
6. M.B. Ali, R. Saidur, M.S. Hossain, Renewable and Sustainable Energy Reviews, 2011, **15**, 2252–2261.
7. M. Bailera, P. Lisbona, L.M. Romeo, S. Espatolero, *Renewable and Sustainable Energy Reviews,* 2017, **69,** 292–312.
8. C. Fukuhara, A. Kamiyama, M. Itoh, N. Hirata, S. Ratchahat, M. Sudoh, R. Watanabe, *Chem Eng Sci*., 2020, **219**,115589.
9. C. Fukuhara, S. Ratchahat, Y. Suzuki, M. Sudoh, R. Watanabe, *Chem Lett.*,2019, **48**, 196–199.
10. L. Dou, C. Yan, L. Zhong, D. Zhang, J. Zhang, X. Li, L. Xiao, *Chemical Communications.*, 2019, **56**, 205–208.
11. J.C. Navarro, M.A. Centeno, O.H. Laguna, J.A. Odriozola, *Renew Energy*., 2020, **161**, 120–132.
12. S. Danaci, L. Protasova, J. Lefevere, L. Bedel, R. Guilet, P. Marty, *Catal Today.*,2016, **273**, 234–243.
13. C. Fukuhara, S. Ratchahat, A. Kamiyama, M. Sudoh, R. Watanabe, *Chem Lett*., 2019, **48**, 441–444.
14. C. Fukuhara, K. Hayakawa, Y. Suzuki, W. Kawasaki, R. Watanabe, *Appl Catal A Gen.*, 2017, **532**, 12–18.
15. S. Renda, A. Ricca, V. Palma, *Int J Hydrogen Energy*, 2021, **46**, 12117-12127.
16. F. Wang, S. He, H. Chen, B. Wang, L. Zheng, M. Wei, D.G. Evans, X. Duan, *J Am Chem Soc*., 2016, **138**, 6298–6305.
17. S. López-Rodríguez, A. Davó-Quiñonero, E. Bailón-García, D. Lozano-Castelló, A. Bueno-López, *Molecular Catalysis*, 2021, **515**, 111911-111920.

Multi-stage spiral-type structured catalyst system for direct large-scale methanation of industrial CO_2 emissions: A feasibility study

Hiroshi Akama[a]*, Ryo Watanabe[a], Priyanka Verma[b], Choji Fukuhara[a,]*

a) *Department of Applied Chemistry and Biochemical Engineering, Graduate School of Engineering, Shizuoka University, 3-5-1 Johoku, Chuo-ku, Hamamatsu, Shizuoka 432-8561*
b) *Department of Chemistry, Indian Institute of Technology Delhi, Hauz Khas, New Delhi – 110016, India*

The data that support the findings of this study are available from the corresponding author, Ryo Watanabe, upon reasonable request.